Leveraging Transdisciplinary Engineering in a Changing and Connected World
P. Koomsap et al. (Eds.)

doi:10.3233/ATDE230604

Translating the Three-Dimensional Mathematical Modelling of Plant Growth to Additive Manufacturing

A. TANSELL[a,1], G. J. LUO[a], L. E. J. THOMAS-SEALE[b] and R. J. DYSON[a]
[a] *School of Mathematics, University of Birmingham, UK*
[b] *Department of Mechanical Engineering, School of Engineering, University of Birmingham, UK*

Abstract. Much like how plants grow via the expansion and multiplication of cells, a 3D printed component is formed via the bonding of material point-by-point from the bottom-up. Exploiting this analogy, this work employs mathematical models of three-dimensional plant growth to further understand and aid implementation of additive manufacturing (AM) technologies (otherwise known as 3D printing). The resolution of these printed structures is of the upmost importance in the fabrication of tissue scaffolds or constructs that mimic the mechanical properties of tissues. As such, the overarching aim is to derive a generalised mathematical model to simulate the extrusion-based bioprinting process via manipulation of the underlying physics of the system. Such a model has the potential to theoretically identify which combinations of printing process parameters generate a successful resolution: the 'window of printability' of a bioink. A hydrogel typically presents a shear-thinning behaviour. In this paper we consider the simplest case: a Newtonian fluid flow far from any edge effects. An initial steady-state model for a viscous thread under extrusion using an arc-length-based coordinate system is presented. As such, this research presents a significant milestone toward representing the non-Newtonian system. This uniquely transdisciplinary methodology seeks to optimise the comparability and transferability of results across materials and laboratories and, above all, increase the efficiency of extrusion-based bioprinting and enhance design creativity by devising a user-friendly, sustainable tool for engineers to visualise AM as a process of growth.

Keywords. Additive Manufacturing, Fluid Mechanics, Transdisciplinary Engineering.

Introduction

Additive manufacturing (AM) is a rapidly advancing technology that presents a far greater design freedom compared to traditional manufacturing methods. It refers to the fabrication process whereby material is placed down in a layer-by-layer fashion to generate three-dimensional (3D) objects (or 'parts') informed directly from computer-aided design model data [1]. This approach generates a vast range of geometric possibilities which are not achievable via traditional manufacturing methods. As such, it can enable geometric optimisation towards a given function (for example, mass) to drive design and generate parts with greater efficiency with respect to the given parameter.

[1] Corresponding Author, Mail: AXT673@student.bham.ac.uk.

Due to the greater design freedom provided by AM, its technologies have been widely employed in tissue engineering, and has adopted the name, '*bioprinting*' [2]. Bioprinting involves the assembly of three-dimensional tissue-like structures via accurate deposition of a bioink (a formulation of encapsulated cells suitable for biofabrication [3]) in a layer-by-layer fashion. Hydrogels and their precursors are commonly used due to their physicochemical properties providing bioink printability and an environment mimicking that of the extracellular matrix that cells are native to [4,5]. Bioprinting and the capacity to create structures that are specific to the geometric requirements of the patient, provides a promising alternative to the fabrication of tissue scaffolds and, thus, emphasises the importance of research into the optimisation of its design strategy [6].

In this paper, we narrow our focus to extrusion-based bioprinting which involves continuous filaments of bioink being pneumatically or mechanically extruded from a cartridge (either tubular or conical in shape) onto a predetermined position on the build platform (as seen in Figure 1). Due to its compatibility with a wide variety of viscosities and the high cell density achieved within the 3D structures produced, extrusion-based bioprinting is the most popular choice of bioprinting method within the literature [7]. However, with cell viability playing a crucial role in the functionality of a tissue, the success of a construct is no longer just dependent on the printability of the material, but on the proportion of healthy cells remaining post-print. Therefore, cell viability adds an additional level of complexity when optimising manufacturing parameters to achieve a successful and reproducable result, compared to fused deposition modelling used in polymer AM [8]. In fact, due to the complex behaviour observed at the mircroscale, obtaining consistent results between applications has proven extremely challenging [9].

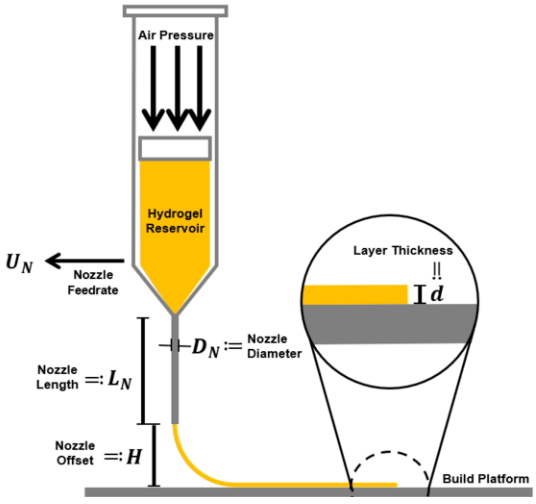

Figure 1. The extrusion-based bioprinting process.

Given the expense and intensity of labour that accompany tissue engineering, future developments involve the generation of quantitative tools and methods to objectively analyse the performance of different bioinks during the extrusion-based bioprinting process. By simulating the process, any experimental analysis and between-laboratory biases can be reduced, aiding the reproducibility of results across the literature and saving time and money [10]. But, due to the non-linear manner with which printing parameters affect the printability of a specific bioink, the problem of predicting and restricting the most influential parameters for a particular application still remains platform- and material-specific. At present, the optimal combination tends to be determined via a print-and-test (characterisation) methodology.

Recent advances have explored the concept of using biological phenomena to inspire new frontiers in manufacturing [11,12]. However, when faced with highly specific challenges, such as the optimisation of bioprinting, the implementation of biological

principles to solve such a problem remains unclear. Although the discipline of transdisciplinary engineering is an emerging research field, Lattanizo *et al.* define transdisciplinarity as the '*transcending of disciplines*' to '*address real-world goals and create societal impact*' [13]. Gooding *et al.* further highlight the importance of this fusing of existing methodologies in the tackling of complex unstructured research problems [14]. In this paper, we present a transdisciplinary approach developed at the interface of biology, engineering, and mathematics. The growth of plants, through the expansion and multiplication of cells, is analogous to the point-by-point bonding of material underpinning fabrication in 3D printing. Utilising this analogy, we approach the optimisation of printing process parameters for bioprinting via the implementation of mathematical principles derived in the modelling of 3D plant growth.

1.1. Optimising Printability of Extrusion-Based Bioprinting

Although a consistent definition is yet to be distinguished throughout the literature, in this paper we shall define the printability of a bioink to be the deviation of a printed construct from the initial 3D model data for a particular application: characterised in terms of extrudability, shape fidelity, and structural integrity [15]. Here, extrudability refers to the capability of a bioink to be continuously extruded through a nozzle in a controlled manner; shape fidelity refers to the difference in cross-sectional area of a filament from that set in the 3D model data; and structural integrity refers to the capability of a construct to hold it's intended structure post-print. We also note that an ideal bioink should exhibit a non-Newtonian behaviour: a shear-thinning property upon extrusion and rapid gelation upon deposition, to aid shape retention.

He *et al.* identified the key printing process parameters necessary to gain precise control of the printability of a gelatin-alginate composite hydrogel via a series of experiments [2]. They determined that the resolution of a printed line of hydrogel is affected by the *nozzle feedrate* (the nozzle moving speed), *nozzle offset* (distance from the tip of the nozzle to the build platform), and *air pressure*. Schwab *et al.* then went on to extend this shortlist by identifying a dependence of these parameters on the *geometry* of the nozzle [16]. Their impact on the resolution of a print was then examined theoretically (and validated experimentally using a Pluronic F-127 hydrogel) by Suntornnond *et al.* via a mathematical model based on the power-law model [17]. Although their work was based in a platform- and material-specific setting, the agreement between the theoretical and experimental results emphasise that mathematical modelling techniques pose a promising alternative to the existing methodology. In fact, empirical modelling techniques are becoming increasingly popular in the literature whilst in the pursuit of a standardised characterisation of bioink printability [18]. That said, with a foundation based on experimental observation, further research is necessary to optimise the comparability and transferability of results generated by empirical models for use across bioinks [19]. We hypothesise that a first-principles modelling approach can be used to overcome this barrier.

By deriving a generalised model based on the non-Newtonian fluid dynamics that underlie the extrusion process – rather than experimental observation – an adaptable quantitative tool usable across platforms and bioinks may be produced. When adjusted to a particular setting, the model has the potential to generate meaningful insights into the rheological profile of the bioink and the complex interconnected relationships between the printing parameters. A consolidation of the data generated by such a model – for varying bioink formulations – has the potential to aid the development of new

materials (and its efficiency) as well as contribute to tackling the challenging problem of achieving high-resolution printing with low viscous materials [20]. Through a sustainability lens, the data could be further exploited to facilitate process monitoring and control methods when examining fabrication and correcting for defects based on process feedback [21].

In this paper, we focus on a slender thread of bioink extruded from a linearly moving nozzle tip onto a stationary build platform and consider the simplest case: a bioink presenting Newtonian fluid flow. We derive a time-dependent system of equations governing the underlying physics of the extrusion process, using an arc-length-based coordinate system. The significance of this milestone in our work towards simulating the non-Newtonian system and our next steps are highlighted.

2. A Mathematical Description of the Extrusion Process

We consider a line of viscous thread being extruded - with a constant and uniform speed u_E - via a nozzle onto a stationary build platform from a height H, as shown in Figure 2. The nozzle moves horizontally with speed U_N. Furthermore, we take μ to be the dynamic viscosity and ρ to be the density of the fluid which is contained within a boundary denoted by $r = R(s, \phi, t)$.

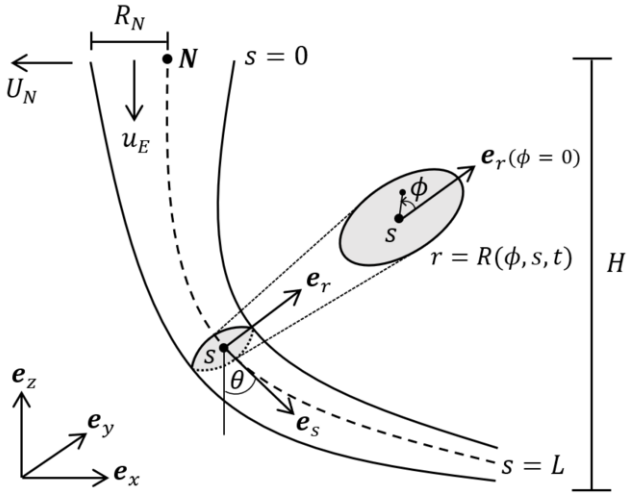

Figure 2. The model set-up, with R_N, U_N, u_E, and H the radius, feedrate, extrusion speed, and offset of the nozzle, respectively. The thread meets the build platform at $s = L$ and the position of the nozzle tip is denoted by $\boldsymbol{N}(t)$ (at $s = 0$). At a chosen s, we have a set of basis vectors $(\boldsymbol{e}_r(\phi, s, t), \boldsymbol{e}_\phi(\phi, s, t), \boldsymbol{e}_s(s, t))$, with $\boldsymbol{e}_s$ pointing in the tangential direction, $\boldsymbol{e}_r$ in the normal direction, and $\boldsymbol{e}_\phi = \boldsymbol{e}_s \times \boldsymbol{e}_r$. An arbitrary point within this cross-section (with radius R) is determined by (r, ϕ, s), with orientation θ from the downward vertical.

Assuming the thread maintains an approximately circular cross-section, the volumetric flow rate Q leaving the nozzle remains constant, taking the value $Q = \pi R_N^2 u_E$, with R_N the radius of the nozzle tip. With the length of the thread being much greater than its thickness, we may assume a slender geometry with a small aspect ratio $\varepsilon = \frac{R_N}{L}$, where L is a typical (and yet to be determined) length of the thread. Exploiting this slenderness, we model the thread via its curved centre-line, parametrised by an arc length s, measured from the nozzle tip to a chosen point, where $\boldsymbol{N}(t) =$

$(N_x(t), N_y(t), H)$ denotes the position of the nozzle tip (at $s = 0$). The point of contact with the build platform can be located at $s = L$. We note that the dynamical properties of the thread can be obtained by taking averages over its cross-section.

2.1. Centre-line Geometry and Kinematics

We denote the position of the centre-line by $\boldsymbol{X}(s,t) = (X(s,t), Y(s,t), Z(s,t))$ – with respect to fixed Cartesian axes (x, y, z) – and assume it lies in the plane $y = 0$. To capture the orientation of the thread, we take $\theta(s,t)$ to be the angle between the tangent at s and the downward vertical. We further define a set of basis vectors $(\boldsymbol{e}_r(\phi,s,t), \boldsymbol{e}_\phi(\phi,s,t), \boldsymbol{e}_s(s,t))$ that move with the flow of the thread, with $\boldsymbol{e}_s$ pointing in the tangential direction (the direction of increasing s), $\boldsymbol{e}_r$ in the normal direction (the direction of increasing r), and $\boldsymbol{e}_\phi = \boldsymbol{e}_s \times \boldsymbol{e}_r$ in the azimuthal direction (the direction of increasing ϕ). Hence, $(\boldsymbol{e}_r, \boldsymbol{e}_\phi)$ rotate around the cross-section at s. By expressing a point within the thread as a linear combination of these unit vectors – that is, with respect to the curved centre-line rather than in general Cartesian space – we significantly reduce the complexity of the mathematics involved in the problem. We assume the thread to be approximately axisymmetric about its centre-line. The variation of the three basis vectors along the centre-line is captured via the curvature of the thread $\kappa(s,t)$ and, assuming the thread remains steady, the centre-line will remain in the plane $y = 0$ and $\kappa(s,t)$ can be expressed as the rate of change of $\theta(s,t)$ with respect to the arc-length s; written mathematically as $\kappa(s,t) = \frac{\partial\theta}{\partial s}$. Therefore, the geometry of the centre-line can be described as follows,

$$\frac{\partial X}{\partial s} = \sin\theta(s,t), \tag{1}$$

$$\frac{\partial Z}{\partial s} = -\cos\theta(s,t), \tag{2}$$

$$\frac{\partial\theta}{\partial s} = \kappa(s,t), \tag{3}$$

and the position of the centre-line may be rewritten as,

$$\begin{aligned}\boldsymbol{r}_c(s,t) = &\left(N_x(t) + \int_0^s \sin\theta(s',t)\,ds'\right)\boldsymbol{e}_x \\ &+ \left(H + \int_0^s -\cos\theta(s',t)\,ds'\right)\boldsymbol{e}_z,\end{aligned} \tag{4}$$

where $N_y(t) = 0$, assuming the centre-line remains in the plane $y = 0$. Equation 4 captures an arbitrary point s along the centre-line from the nozzle tip $\boldsymbol{N}$ (where $s = 0$) in Cartesian space. We note that we obtain the tangential basis vector $\boldsymbol{e}_s$ when we differentiate $\boldsymbol{r}_c(s,t)$ with respect to s, given by,

$$\boldsymbol{e}_s = \frac{\partial \boldsymbol{r}_c}{\partial s} = \sin\theta\,\boldsymbol{e}_x - \cos\theta\,\boldsymbol{e}_z. \tag{5}$$

While the associated basis vectors in the radial and azimuthal directions can be written as,

$$\boldsymbol{e}_r = \cos\theta\cos\phi\,\boldsymbol{e}_x - \sin\phi\,\boldsymbol{e}_y + \sin\theta\cos\phi\,\boldsymbol{e}_z, \tag{6}$$

$$\boldsymbol{e}_\phi = -\cos\theta\sin\phi\,\boldsymbol{e}_x - \cos\phi\,\boldsymbol{e}_y - \sin\theta\sin\phi\,\boldsymbol{e}_z, \tag{7}$$

where,

$$\boldsymbol{e}_x = \cos\theta\cos\phi\,\boldsymbol{e}_r - \cos\theta\sin\phi\,\boldsymbol{e}_\phi + \sin\theta\,\boldsymbol{e}_s, \tag{8}$$

$$\boldsymbol{e}_y = -\sin\phi\,\boldsymbol{e}_r - \cos\phi\,\boldsymbol{e}_\phi, \tag{9}$$

$$\boldsymbol{e}_z = \sin\theta\cos\phi\,\boldsymbol{e}_r - \sin\theta\sin\phi\,\boldsymbol{e}_\phi - \cos\theta\,\boldsymbol{e}_s. \tag{10}$$

Here, an arbitrary point in Cartesian space is defined by,

$$x = N_x(t) + \int_0^s \sin\theta(s',t)\,ds' + r\cos\theta\cos\phi, \tag{11}$$

$$y = -r\sin\phi, \tag{12}$$

$$z = H + \int_0^s -\cos\theta(s',t)\,ds' + r\sin\theta\cos\phi, \tag{13}$$

with r the radial coordinate in the $\boldsymbol{e}_r$ direction and ϕ the angle in the $\boldsymbol{e}_\phi$ direction (lying in the cross-section at s). Equations 11 to 13 relate the 'old' coordinates (x, y, z) to our 'new' arc-length-based coordinates (r, ϕ, s). The origin is taken to be the position of the nozzle tip $\boldsymbol{N}(t) = (N_x(t), 0, H)$, captured via the first terms of Equations 11 and 13. Since the centre-line lies in the plane $y = 0$, only x and z depend on s, which increase along the centre-line, and this is captured in the second terms of Equations 11 and 13. Any displacement from this plane (a point within the cross-section of the thread at a fixed s) is captured via the third terms in Equations 11 and 13, and the y expression now takes on a non-zero value. We note that when we set $r = 0$, we return to a point on the centre-line (as expressed in Equation 4).

We may define the rate of change of position of the centre-line (stated in Equation 4) as follows,

$$\frac{\partial \boldsymbol{r}_c}{\partial t} = v_r(\phi, s, t)\,\boldsymbol{e}_r + v_\phi(\phi, s, t)\,\boldsymbol{e}_\phi + v_s(s, t)\,\boldsymbol{e}_s, \tag{14}$$

where $\boldsymbol{v} = (v_r, v_\phi, v_s)$ denotes the velocity of the centre-line.

2.2. The Dimensional Equations Capturing the Fluid Flow

In Section 2.1 we devised a means to describe the geometry and motion of the thread with respect to some fixed frame of reference – but this is only part of the dynamics – we must also model the fluid flow within the thread (with respect to the centre-line). The velocity of the fluid is denoted by $\boldsymbol{u} = (u_r, u_\phi, u_s)$ and its flow is characterised by a balance of mass and momentum captured via the *Conversation of Momentum* and

Conservation of Mass equations. Therefore, the time-dependent system governing the fluid flow within a thread under extrusion in our arc-length-based coordinate system is given by: the s-component of conservation of momentum,

$$\begin{aligned}\rho\Bigg(&\frac{\partial}{\partial t}(u_s+v_s)+(u_r+v_r)\frac{\partial u_s}{\partial r}+\frac{(u_\phi+v_\phi)}{r}\frac{\partial u_s}{\partial \phi}+\frac{(u_s+v_s)}{L_s}\frac{\partial u_s}{\partial s}\\&+\frac{\kappa(u_s+v_s)}{L_s}\big(\sin\phi\,u_\phi-\cos\phi\,u_r\big)\Bigg)\\=&\frac{\partial \sigma_{sr}}{\partial r}+\frac{1}{r}\frac{\partial \sigma_{s\phi}}{\partial \phi}+\frac{1}{L_s}\frac{\partial \sigma_{ss}}{\partial s}+\frac{\sigma_{sr}}{r}-\frac{2\kappa}{L_s}\big(\cos\phi\,\sigma_{sr}-\sin\phi\,\sigma_{s\phi}\big)\\&+\rho g\cos\theta\,;\end{aligned}\tag{15}$$

the ϕ-component of conservation of momentum,

$$\begin{aligned}\rho\Bigg(&\frac{\partial}{\partial t}\big(u_\phi+v_\phi\big)+(u_r+v_r)\frac{\partial u_\phi}{\partial r}+\frac{(u_\phi+v_\phi)}{r}\frac{\partial u_\phi}{\partial \phi}+\frac{(u_s+v_s)}{L_s}\frac{\partial u_\phi}{\partial s}\\&+\frac{u_r\big(u_\phi+v_\phi\big)}{r}-\frac{\sin\phi\,(u_s+v_s)}{L_s}\Big(\kappa\,u_s+\frac{\partial\theta}{\partial t}\Big)\Bigg)\\=&\frac{\partial \sigma_{\phi r}}{\partial r}+\frac{1}{r}\frac{\partial \sigma_{\phi\phi}}{\partial \phi}+\frac{1}{L_s}\frac{\partial \sigma_{\phi s}}{\partial s}+\frac{2\sigma_{\phi r}}{r}+\frac{\kappa}{L_s}\big(\sin\phi\,(\sigma_{\phi\phi}-\sigma_{ss})\\&-\cos\phi\,\sigma_{\phi r}\big)+\rho g\sin\theta\sin\phi\,;\end{aligned}\tag{16}$$

and the r-component of conservation of momentum,

$$\begin{aligned}\rho\Bigg(&\frac{\partial}{\partial t}(u_r+v_r)+(u_r+v_r)\frac{\partial u_r}{\partial r}+\frac{(u_\phi+v_\phi)}{r}\frac{\partial u_r}{\partial \phi}+\frac{(u_s+v_s)}{L_s}\frac{\partial u_r}{\partial s}\\&-\frac{u_\phi\big(u_\phi+v_\phi\big)}{r}+\frac{\cos\phi\,(u_s+v_s)}{L_s}\Big(\kappa\,u_s+\frac{\partial\theta}{\partial t}\Big)\Bigg)\\=&\frac{\partial \sigma_{rr}}{\partial r}+\frac{1}{r}\frac{\partial \sigma_{r\phi}}{\partial \phi}+\frac{1}{L_s}\frac{\partial \sigma_{rs}}{\partial s}+\frac{\sigma_{rr}-\sigma_{\phi\phi}}{r}+\frac{\kappa}{L_s}\big(\cos\phi\,(\sigma_{ss}-\sigma_{rr})\\&+\sin\phi\,\sigma_{r\phi}\big)-\rho g\sin\theta\cos\phi\,;\end{aligned}\tag{17}$$

and a conservation of mass,

$$\rho\left(\frac{u_r}{r}+\frac{\partial u_r}{\partial r}+\frac{1}{r}\frac{\partial u_\phi}{\partial \phi}+\frac{1}{L_s}\frac{\partial u_s}{\partial s}-\frac{\kappa}{L_s}\big(\cos\phi\,u_r-\sin\phi\,u_\phi\big)\right)=0,\tag{18}$$

where $\boldsymbol{\sigma}$ denotes the stress tensor (with components σ_{ij}, where i and j range over r, ϕ, and s), g gravitational acceleration, and $L_s=1-r\kappa\cos\phi$ (a scaling factor). Equations 15 to 18 are subject to the following initial conditions:

$$u_i(r,\phi,s,t)=0,\qquad \text{at}\quad r=0,\quad \text{for}\quad i=r,\phi;\tag{19}$$

as well as those imposed by the bioprinter set-up itself,

$$R(\phi, s, t) = R_N, \tag{20}$$

$$u_s(r, \phi, s, t) = u_E, \tag{21}$$

$$\theta(s, t) = 0, \tag{22}$$

at $s = 0$. Furthermore, since the cross-section of the thread is approximately circular, we must have that the pressure and fluid velocity at $\phi = 0$ are the same as that at $\phi = 2\pi$, written mathematically as,

$$\begin{aligned} &p(r, 0, s, t) = p(r, 2\pi, s, t), \\ &u_i(r, 0, s, t) = u_i(r, 2\pi, s, t), \\ &\frac{\partial u_i}{\partial \phi}(r, 0, s, t) = \frac{\partial u_i}{\partial \phi}(r, 2\pi, s, t), \qquad \text{for} \quad i = r, \phi, s. \end{aligned} \tag{23}$$

Finally, we impose two boundary conditions at $r = R$: a kinematic boundary condition, stating that if a fluid particle starts on the boundary it will remain on the boundary; and a no-stress boundary condition, arising from a force balance between stress and surface tension, having assumed the surface tension negligible for mathematical simplicity. It is noted that the assumption of a constant and uniform extruson velocity u_E is necessary to ensure continuity of the no-stress boundary condition at the nozzle tip.

We have generated four equations satisfied by ten unknowns describing the motion of the thread under extrusion: the fluid velocity with respect to the centre-line u_i (for $i = r, \phi, s$); the velocity of the centre-line v_i (for $i = r, \phi, s$); the radius of the cross-section R; the orientation of the thread θ; the hydrostatic pressure of the fluid p (captured in the stress tensor); and the length of the thread L. Thus, with more unknowns than equations, the system remains underdetermined and we must manipulate the system in such a way to arrive at a closed system[2] that can be solved. Due to the non-linear nature of the equations involved, a closed system may be achieved via a combination of asymptotic and other simplifying methods, from which an approximation to the solution is obtained.

3. Limitations and Future Developments

The print resolution of a bioink is dependent on the cross-sectional area of the thread, therefore, the primary unknown of interest for this problem is the radius of the printed thread R (at $s = L$). Our future work involves the use of a combination of asymptotic and other simplifying methods to reduce the currently underdetermined system (given by Equations 15 to 23) to a closed system. Once solved, information on the variation of R as the thread is extruded, from the nozzle tip to the point it touches the build platform, will be obtained. When adjusted to a particular setting, the results of the model will provide meaningful insight into the rheological profile of the bioink and the complex interconnected relationships between the printing process parameters. Thus, use of the model prior to printing can provide the user with a more precise 'window of printability' of the bioink, reducing the number of prints necessary to obtain a optimal resolution, when compared to the current print-and-test methodology [19].

[2] A system consisting of the same number of equations as unknowns.

In addition to aiding AM in its aim towards a sustainable future, the foundations of the model derivation provides this work with an upper hand over existing empirical modelling approaches currently in the literature. By not assuming a specific platform and material and instead exploiting the underlying physics of the extrusion process – rather than experimental observation – any potential between-material and between-laboratory biases are greatly reduced. Hence, a compilation of model data in different settings could further optimise the efficiency of process parameter definition within the design workflow, providing users with an initial approximation for the 'window of printability' prior to applying the model to their own setting.

The model presented assumes a Newtonian, incompressible fluid flow and neglects surface tension and temperature effects. Although an ideal bioink presents a shear-thinning property upon extrusion and rapid gelation upon deposition, with filament formation impacted by surface tension, the 'simplest' case considered in this work remains an important milestone in our work towards the non-Newtonian model; providing us with a strong initial framework upon which non-Newtonian extensions can build. With this framework in place, we can then begin to relax our assumptions on surface tension, by relaxing the boundary condition at $r = R$, moving from a no-stress condition used in this work to a force balance between stress and surface tension, and the viscosity μ, by considering in silico models such as the Herschel-Bulkley model to capture the expected non-Newtonian fluid flow and temperature effects [22,23]. By iteratively relaxing each assumption in turn enables the model to gradually converge towards the real system as well as provide any justification for effects assumed negligible in the modelling process. It is noted that since the methodology used requires simplifications and assumptions we intend to employ experimental techniques to provide validation at each milestone.

4. Conclusion

The transdisciplinary approach taken in this paper has transposed mathematical approaches associated with 3D plant growth to a new application in manufacturing engineering. This has enabled the implementation of a biological analogy and, subsequently, the derivation of a robust methodology with the purpose to ease the complexity of defining process parameters in the design workflow for extrusion-based bioprinting. Exploiting the underlying fluid dynamics of the extrusion of a slender viscous thread, we derived a generalised mathematical model that, upon further manipulation, can be solved to characterise the print resolution. This analytical approach optimises the comparability and transferability of results across materials and laboratories and, above all, increases the efficiency of extrusion-based bioprinting and enhances design creativity by devising a user-friendly, sustainable tool for engineers to visualise the complex AM process as a process of growth.

Acknowledgement

This work was supported by the UK Engineering and Physical Sciences Research Council (EPSRC) Grant EP/S02297X/1 for the University of Birmingham Centre for Doctoral Training in Topological Design.

References

[1] A. Gebhardt, *Understanding Additive Manufacturing*, Hanser Publishers, Munich, 2011.

[2] Y. He, F. Yang, H. Zhao, Q. Gao, B. Xia, and J. Fu, Research on the Printability of Hydrogels in 3D Bioprinting, *Sci. Rep.*, 2016, Vol 6, 29977.

[3] J. Groll, J.A. Burdick, D.-W. Cho, B. Derby, M. Gelinksky, S.C. Heilshorn, T. Jüngst, J. Malda, V.A. Mironov, K. Nakayama, A. Ovsianikov, W. Sun, S. Takeuchi, J.J. Yoo, and T.B.F. Woodfield, A Definition of Bioinks and their Distinction from Biomaterial Inks, *Biofabrication*, 2019, Vol 11, 013001.

[4] M. Chopin-Doroteo, E.A. Mandujano-Tinoco, and E. Krötzsch, Tailoring of the Rheological Properties of Bioinks to Improve Bioprinting and Bioassembly for Tissue Replacement, *BBA - General Subjects*, 2021, Vol 1865, 129782.

[5] G. Gillispie, P. Prim, J. Copus, J. Fisher, A.G. Mikos, J.J. Yoo, A. Atala, and S.J. Lee, Assessment Methodologies for Extrusion-Based Bioink Printability, *Biofabrication*, 2020, Vol 12, 022003.

[6] J.M. Lee and W.Y. Yeong, Design and Printing Strategies in 3D Bioprinting of Cell-Hydrogels: A Review, *Adv. Healthc. Mater.*, 2016, Vol 5, pp. 2856–2865.

[7] S. Ramesh, O.L.A. Harrysson, P.K. Rao, A. Tamayol, D.R. Cormier, Y. Zhang, and I.V. Rivero, Extrusion Bioprinting: Recent Progress, Challenges, and Future Opportunities, *Bioprinting*, 2021, Vol 21, e00116.

[8] O.A. Mohamed, S.H. Masood, and J.L. Bhowmik, Optimization of Fused Deposition Modeling Process Parameters: A Review of Current Research and Future Prospects, *Adv. Manuf.*, 2015, Vol 3, pp. 42–53.

[9] E.N. Udofia and W. Zhou, A Guiding Framework for Microextrusion Additive Manufacturing, *J. Manuf. Sci. Eng.*, 2019, Vol 141, 050801.

[10] J. Göhl, K. Markstedt, A. Mark, K. Håkansson, P. Gatenholm, and F. Edelvik, Simulations of 3D Bioprinting: Predicting Bioprintability of Nanofibrillar Inks, *Biofabrication*, 2018, Vol 10, 034105.

[11] G. Byrne, D. Dimitrov, L. Monostori, R. Teti, F. van Houten and R. Wertheim, Biologicalisation: Biological Transformation in Manufacturing, *CIRP J. Manuf. Sci. Technol.*, 2018, Vol 21, pp. 1–32.

[12] L.E.J. Thomas-Seale, J.C. Kirkman-Brown, S. Kanagalingam, M.M. Attallah, D.M. Espino and D.E.T. Shephard, The Analogies Between Human Development and Additive Manufacture: Expanding the Definition of Design, *Cogent Eng.* , 2019, Vol 6, DOI: 10.1080/23311916.2019.1662631.

[13] S. Lattanzio, L. Newnes, G. Parry, and A. Nassehi, Concepts of Transdisciplinary Engineering: A Transdisciplinary Landscape, *Int. J. Agile Syst. Manag.*, Vol 14, 2021, pp. 292-312.

[14] H. Gooding, S. Lattanzio, G. Parry, L. Newnes and E. Alpay, Characterising the Transdisciplinary Research Approach, *Product: Management and Development*, 2022, Vol 20, e20220012.

[15] Z. Fu, S. Naghieh, C. Xu, C. Wang, W. Sun, and D.X. Chen, Printability in Extrusion Bioprinting, *Biofabrication*, 2021, Vol 13, 033001.

[16] A. Schwab, R. Levato, M. D'Este, S. Piluso, D. Eglin, and J. Malda, Printability and Shape Fidelity of Bioinks in 3D Bioprinting, *Chem. Rev.*, 2020, Vol 120, pp. 10850–10877.

[17] R. Suntornnond, E.Y.S. Tan, J. An, and C.K. Chua, A Mathematical Model on the Resolution of Extrusion Bioprinting for the Development of New Bioinks, *Materials*, 2016, Vol 9, 756.

[18] S. Naghieh and X. Chen, Printability – A Key Issue in Extrusion-Based Bioprinting, *J. Pharm. Anal.*, 2021, Vol 11, pp. 564–579.

[19] N. Paxton, W. Smolan, T. Böck, F. Melchels, J. Groll, and T. Jungst, Proposal to Assess Printability of Bioinks for Extrusion-Based Bioprinting and Evaluation of Rheological Properties Governing Bioprintability, *Biofabrication*, 2017, Vol 9, 044107.

[20] K. Hölzl, S. Lin, L. Tytgat, S.V. Vlierberghe, L. Gu, and A. Ovsianikov, Bioink Properties Before, During and After 3D Bioprinting, *Biofabrication*, 2016, Vol 8, 032002.

[21] A.A. Armstrong, A. Pfeil, A.G. Alleyne, and A.J. Wagoner Johnson, Process Monitoring and Control Strategies in Extrusion-Based Bioprinting to Fabricate Spatially Graded Structures, *Bioprinting*, 2021, Vol 21, e00126.

[22] M. Sarker and X.B. Chen, Modeling the Flow Behavior and Flow Rate of Medium Viscosity Alginate for Scaffold Fabrication with a Three-Dimensional Bioplotter, *J. Manuf. Sci. Eng.*, 2017, Vol 139, 081002.

[23] X.Y. Tian, M.G. Li, N. Cao, J.W. Li, and X.B. Chen, Characterization of the Flow Behavior of Alginate/Hydroxyapatite Mixtures for Tissue Scaffold Fabrication, *Biofabrication*, 2009, Vol 1, 045005.